metals

MDPI

Article

Preparation and Energy Release Properties of nB@F2603@CL-20 Microspheres by Electrospray

Jie Yao, Yanjie Huang, Kanghua Chang, Jianxin Nie, Xueyong Guo, Chen Shen * and Shi Yan *

State Key Laboratory of Explosion Science and Technology, Beijing Institute of Technology, Beijing 100081, China
* Correspondence: shenchen1638@163.com (C.S.); bityanshi@126.com (S.Y.)

Abstract: Nano-boron, as a potential high-energy additive due to its high calorific value, is widely studied in propellants, explosives, and thermites. However, the unexpected agglomeration of surface oxidation hinders its further application, especially in the casting of energetic materials. The fluorine-modified nano-boron nB@F2603 and nB@F2603@CL-20 preagglomerated microspheres were prepared by electrospray to improve the ignition and combustion reactions and the rheological properties of boron-containing casting systems. Sphericity microspheres could be obtained by controlling the voltage and propulsion rate. The morphology and elemental distribution of the microspheres were characterized by the scanning electron microscope (SEM), energy-dispersive X-ray spectroscopy (EDS), and X-ray diffractometer (XRD). Results showed that the particle size of the microspheres ranged from 4 to 14 μm. Boron, fluorine and nitrogen were uniformly distributed on the surface of the microspheres. XRD results showed that CL-20 in nB@F2603@CL-20 microspheres was β-crystal. The thermal reaction properties were studied by differential scanning calorimetry, thermogravimetry and mass spectrometry (TG-DSC-MS), oxygen bomb calorimeter, laser ignition, and volume combustion cell test. Results showed that F2603 could significantly promote the ignition and combustion of nano-boron, causing higher energy release and pressurization rates, and lower ignition temperature. Adding CL-20 to the microspheres could also greatly promote the reaction rates and energy release. The hydrophobicity and corrosion resistance of the structures were also studied, and results showed that the preagglomerated microspheres had good stabilities. Therefore, fluorine-containing nB@F2603 and nB@F2603@CL-20 microspheres might be used in composite energetic materials, replacing nano-boron.

Keywords: nano-boron; energetic materials; electrospray; microsphere; ignition and combustion

check for updates

Citation: Yao, J.; Huang, Y.; Chang, K.; Nie, J.; Guo, X.; Shen, C.; Yan, S. Preparation and Energy Release Properties of nB@F2603@CL-20 Microspheres by Electrospray. *Metals* **2022**, *12*, 1727. https://doi.org/10.3390/met12101727

Academic Editor: Leonid M. Kustov

Received: 15 September 2022
Accepted: 13 October 2022
Published: 15 October 2022

Publisher's Note: MDPI stays neutral with regard to jurisdictional claims in published maps and institutional affiliations.

Copyright: © 2022 by the authors. Licensee MDPI, Basel, Switzerland. This article is an open access article distributed under the terms and conditions of the Creative Commons Attribution (CC BY) license (https://creativecommons.org/licenses/by/4.0/).

1. Introduction

High-energy additives are one of the ways to realize high energy of energetic materials. The mass calorific value of boron is 58.74 MJ/kg, and the volume calorific value is 135.24 kJ/cm^3, making it the most potential high-energy additives in energetic materials [1,2]. However, boron is an atomic crystal with high melting and boiling points, which make it difficult to ignite boron powder [3]. In the reaction process of energetic materials, boron is not easy to melt and vaporize, and the combustion reaction is dominated by layer-by-layer combustion with a slow rate [4]. As the combustion reaction progresses, the thickness of this oxide layer increases continuously; this hinders the contact between boron and oxygen, resulting in the insufficient combustion of boron and a low energy release rate [5]. A large number of theoretical and experimental studies have been conducted to address these problems. Metal powders with low melting points and high calorific values are added to promote the combustion and ignition of boron. These metal powders such as Al, Mg, Ti, and so on [6–8], can be ignited at a lower temperature and release higher energy, which not only promotes the advance combustion of boron powders but also reduces the surface oxide layer to B and metal oxides, thereby improving the activity of boron. The surface of boron is also coated to improve the activity, ignition, and combustion of boron powder [9–11]. When the surface of boron is coated with fluorine rubber,

fluorine-containing fragments react with the surface oxide layer (B_2O_3), thereby improving the activity, ignition, and combustion of boron powder [11].

The particle size of high-energy additives has a considerable influence on the energy density of energetic materials. Reducing the powder particle size can significantly improve the combustion rate and energy release efficiency of powders [1]. Compared with micron-sized particles, nanoparticles have a lower ignition temperature, stronger heat and mass transfer performance, lower sintering temperature, and better overall combustion characteristics [1,12–14]. However, nano-boron powder has a large specific surface area, an easily oxidized surface, and high viscosity, which lead to easy agglomeration, insufficient combustion, and poor mechanical properties [15]. These problems are addressed by assembling n-B into micron-sized structures in a manner that maintains their original properties.

Electrospray is a method of dispersing, atomizing, and depositing a liquid solution into ultrafine particles by a high-voltage electrostatic field. Compared with the high-energy materials prepared via traditional physical mixing, those obtained by the electrospray method have regular morphologies and uniform sizes, thus exhibiting better combustion performance. Binders can increase the contact area between components, reduce the mass transfer distance, improve the agglomeration and oxidation of nanoparticles, and enhance the reactivity of composite particles [16–20]. Therefore, the selection of binders is of great significance for the energy release of energetic materials. For a boron-based energetic system, fluorine-containing polymers are good binders because they can react with the oxide layer on the boron surface to form BF3 due to the fluorine-containing fragments released by their decomposition, thereby improving the reactivity of boron powder [21]. Fluororubber F2603 is an elastomer polymerized by hexafluoropropylene (HFP) and vinylidene fluoride (VDF). Compared with other types of fluoropolymers, F2603 has a higher fluorine content and better thermal conductivity, which can promote fluoride reaction and heat transfer on the surfaces of boron nanoparticles. Hexanitrohexaazaisowurtzitane (CL-20) is currently the highest-energy single compound explosive [22] added into the system to improve the ignition and combustion of n-B.

In this study, n-B, F2603, and CL-20 were assembled into nB@F2603@CL-20 microspheres by the electrospray method. F2603 was introduced into the precursor solution as both the coating agent of n-B and the binder for the electrospray process. The binder could not only adjust the final particle size and morphology but also improve the ignition and combustion properties of n-B. The addition of CL-20 significantly enhanced the combustion characteristics of the microspheres. The combustion behavior of the nB@F2603@CL-20 microspheres was systematically evaluated through an ignition experiment and a constant-volume combustion chamber. The results showed that the nB@F2603@CL-20 microspheres exhibited stronger energy release characteristics than boron nanoparticles and nB@F2603 microspheres.

2. Experimental Section

2.1. Materials

Boron nanoparticles (n-B) sized 45–55 nm were purchased from Shanghai Xiangtian Nanomaterials Co., Ltd., Shanghai, China. The active content of n-B from the supplier was 76% by mass, as determined by thermogravimetric (TG) analysis. CL-20 was provided by Liaoning Qingyang Chemical Industry Co., Ltd., Liaoyang, China. F2603 (71% fluoride content) was obtained from Bluestar Chengrand Co., Beijing, China. Ethyl acetate was purchased from Beijing Tongguang Fine Chemical Co., Beijing, China. All chemicals were used as received.

2.2. Preparation of Compound Microspheres

Typically, 400 mg of solid mixture consisting of 320 mg n-B, 40 mg CL-20, and 40 mg F2603 was added to 2 mL ethyl acetate. The mixture was stirred vigorously for 24 h to ensure complete dissolution of F2603 and CL-20. Afterward, the mixture was ultrasonically sonicated for 1 h and then subsequently continuously stirred for 24 h to form a homogeneous precursor solution. Finally, this precursor solution was electrosprayed by an

electrostatic spray setup (Elite, Beijing Yongkang Leye Technology Development Co., Ltd., Beijing, China). The homogeneous suspension was loaded into an injector with a no. 20 stainless steel nozzle. The nozzle tip and the substrate (aluminum foil) were kept 15 cm apart to ensure the formation of dry particles. The nozzle and the substrate were maintained at +14 and −1 kV, respectively. The electrospray process was completed at 25 °C, and the solution flowed out of the nozzle at a speed of 0.29 mm·min^{-1}. The electrospray preparation process is shown in Figure 1.

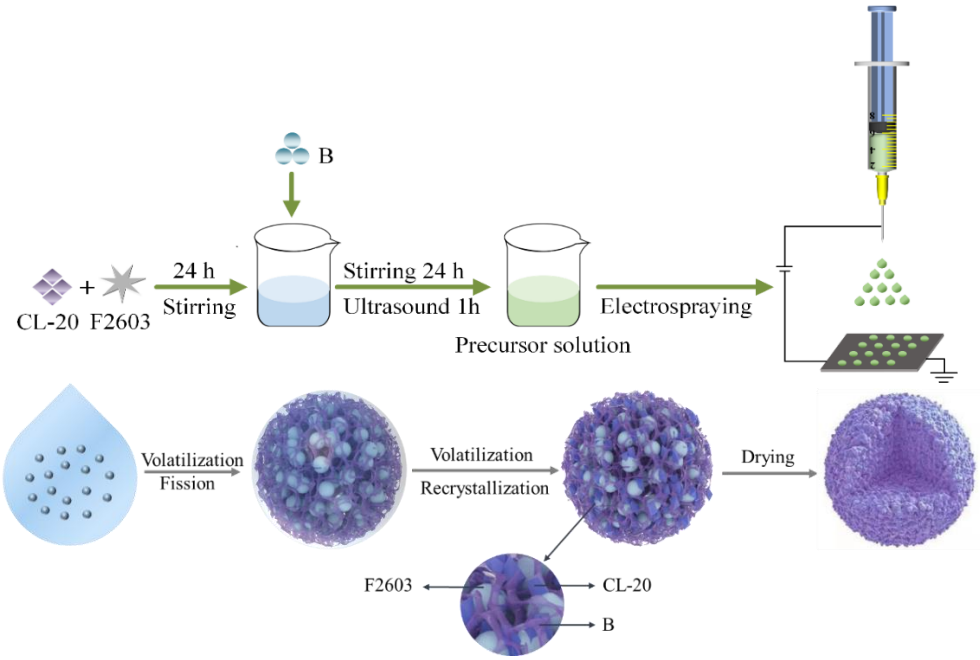

Figure 1. Schematic of electrospray process.

2.3. Characterization

2.3.1. Morphological Characteristics

The morphologies and element distributions of the samples were analyzed by scanning electron microscopy (SEM; S-4800, Hitachi, Tokyo, Japan) coupled with energy-dispersive X-ray spectroscopy (EDS). The crystal phases of raw CL-20, nB@F2603 microspheres, and nB@F2603@CL-20 microspheres were examined by X-ray diffraction (XRD) with Cu Ka radiation (D8 Advance, Bruker, Werder Bremen, Germany). The particle size distributions of the nB@F2603 and nB@F2603@CL-20 microspheres were measured with a Malvern Mastersizer 2000 (Malvern, Malvern City, UK).

2.3.2. Hydrophobic and Acid Corrosion Resistance

The static water contact angles (WCAs) of n-B, F2603, and the nB@F2603 microspheres were measured at room temperature using an optical contact angle measuring device (Biolin Ltd., Sweden, Switzerland), and 2 µL deionized water droplets were used each time. Each sample was tested at different locations five times to obtain an average value. Since n-B is relatively stable at room temperature, n-Al with the same particle size, which was assembled into microspheres by electrospray, was used in place of n-B to verify the corrosion resistance of the nB@F2603 microsphere structure. Then, 100 mg of each sample was added to a 300 mL HCl solution for 10 min. The remaining samples were collected, washed, dried, and weighed to calculate the weight percentages of residual n-B. The experiment was conducted three times to reduce errors.

2.3.3. Thermal Analysis

Thermal analysis was conducted on n-B, and nB@F2603 microspheres and nB@F2603@CL-20 microspheres at different heating rates (5 °C/min, 10 °C/min, 15 °C/min, and 20 °C/min) in air from 25 °C to 1200 °C at a flow rate of 50 mL/min using TG analysis, differential scanning calorimetry (DSC) and micro-quotient thermogravimetric analysis (DTG) (TG-DSC-DTG; Netzsch STA 449F3, Selb, Germany). The nB@F2603@CL-20 microspheres were analyzed by TG mass spectrometry (TG-DTA-MS). About 4 mg of each sample was heated at a heating rate of 10 K/min in Ar from room temperature to 1000 °C at a flow rate of 50 mL/min.

2.3.4. Ignition and Combustion Performance

The heat during the combustion of the microspheres was evaluated using a micro-computer automatic calorimeter (MAC; TRHW-7000C, Hebi Tianrun Electronic Technology Co., Ltd., Hebi, China). About 200 mg of each sample was placed on the sample stage of the calorimeter, and the calorimeter was sealed. The sample was ignited by adding 3 MPa oxygen to the calorimeter and heating it with a Ni–Cr alloy wire. The heat released by the reaction was dispersed into the water bath in the calorimeter, which caused the system temperature to rise, and the combustion heat of the sample was determined. Each sample was measured three times, and the results were averaged.

The reaction performance of the samples was characterized through a constant-volume combustion cell test. Approximately 50 mg of each sample was weighted and loaded into a combustion cell with a constant-volume of about 50 cm^3. The sample was subjected to Joule heating and ignited using the Ni–Cr alloy wire. Afterward, the sample was lit, and a pressure sensor was used to record the pressure change over time.

Each sample was ignited using a CO_2 laser, and the ignition was recorded by a high-speed camera (Qianlilang X113, Qianlilang, Beijing, China) at 10,000 frames per second. The energy provided by the laser depended on the laser power and ignition time. A total of 30% ammonium perchlorate (AP) was added to each sample to ensure the strength and proper recording of its combustion. About 20 mg powder was placed at the center of the stage and ignited in air. The time on each image in the figure represents the flame propagation process of the trigger signal. The time of the first spark was recorded as 0 ms. Ignition was considered to have occurred when the radiation intensity was the highest. Ignition delay was defined as the time period from the beginning of laser ignition to the appearance of the first visible spark captured by the high-speed camera. The laser ignition test platform is a customized build platform. TheSchematic diagram of laser ignition platform is shown in Figure 2.

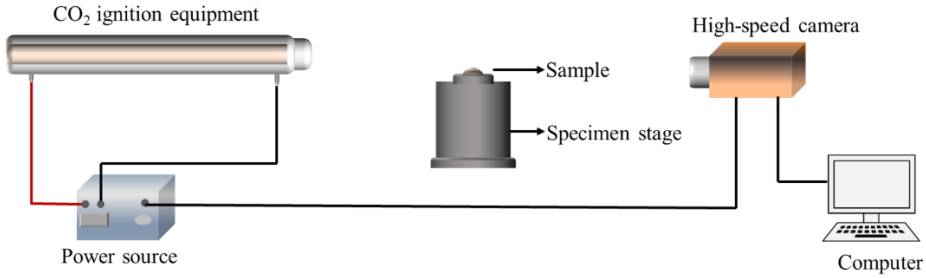

Figure 2. Schematic diagram of laser ignition platform.

3. Results and Discussion

3.1. Morphology and Component Analysis

Figure 3 shows the SEM images of the nB@F2603 and nB@F2603@CL-20 microspheres, which are well-dispersed and exhibit highly spherical morphology. The surfaces of the microspheres have many holes. The elemental analysis results show that the elements B, F, and N are evenly distributed in the microspheres, as shown in Figure 4. Therefore, n-B, F2603, and CL-20 are successfully assembled into the microspheres. The particle sizes of the nB@F2603 and nB@F2603@CL-20 microspheres are measured by the Malvern Mastersizer

2000, as shown in Figure 5a. The particle sizes of the nB@F2603 and nB@F2603@CL-20 microspheres are between 4 and 14 μm. Figure 5b presents the crystal form of CL-20 in the nB@F2603@CL-20 microspheres. According to the XRD patterns of pure ε-CL-20 and β-CL-20 (PDF card numbers 050-2045 and 052-2432, respectively), raw CL-20 has an ε crystal form, whereas the CL-20 recrystallized during electrospray has a β crystal form, which is consistent with the results in the literature [23].

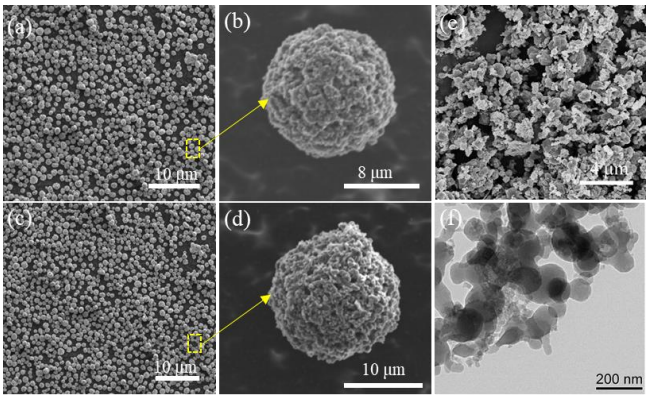

Figure 3. SEM images of (**a**,**b**) nB@F2603, (**c**,**d**) nB@F2603@CL-20 microspheres, and nB (**e**); TEM images of nB (**f**).

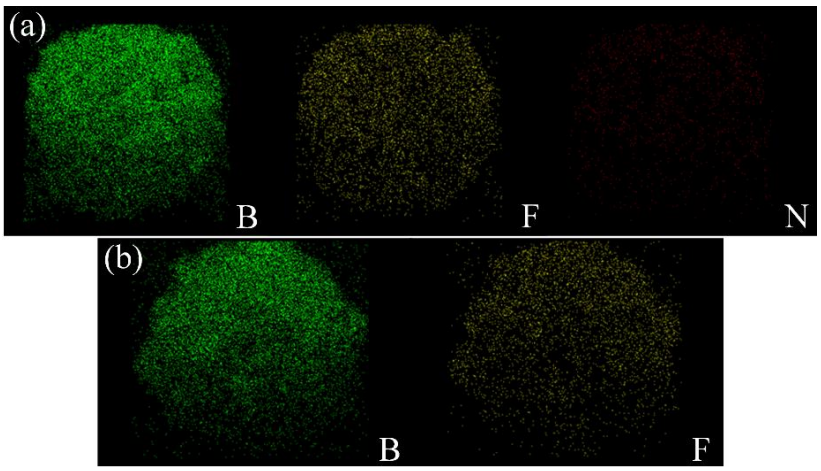

Figure 4. EDS elemental mapping of (**a**) nB@F2603@CL-20 and (**b**) nB@F2603 microspheres.

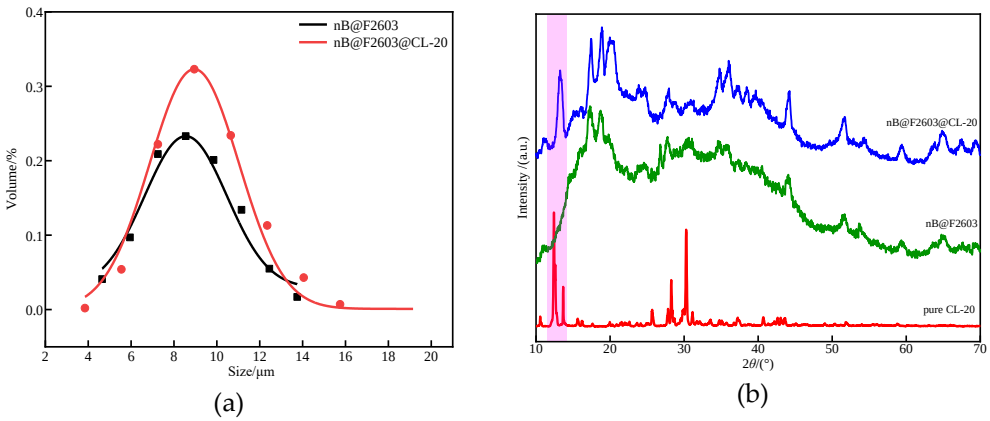

Figure 5. (**a**) Particle size distribution and (**b**) XRD patterns of nB@F2603@CL-20 microspheres.

3.2. Hydrophobicity and Corrosion Resistance

The hydrophobicity of n-B and the nB@F2603 microspheres was evaluated by the WCA test. Figure 6a shows that the deionized water spreads throughout the n-B surface rapidly after being dropped, with a final WCA of about 10.4°. This is due to n-B and the natural oxide layer on its surface. Figure 6b shows that the WCA of the pure F2603 film is about 108.7°, which proves its hydrophobicity. Figure 6f shows that the irregularly pleated polymer layer (F2603) tightly adhered to the surface of the nB particles. Because of this special structure formed, the microspheres have a certain hydrophobicity. The WCA of the nB@F2603 microspheres is 98.5°, which is slightly lower than that of the pure F2603 film. This is because part of the n-B in the microspheres is not completely wrapped by F2603; the high-energy microspheres are still hydrophobic.

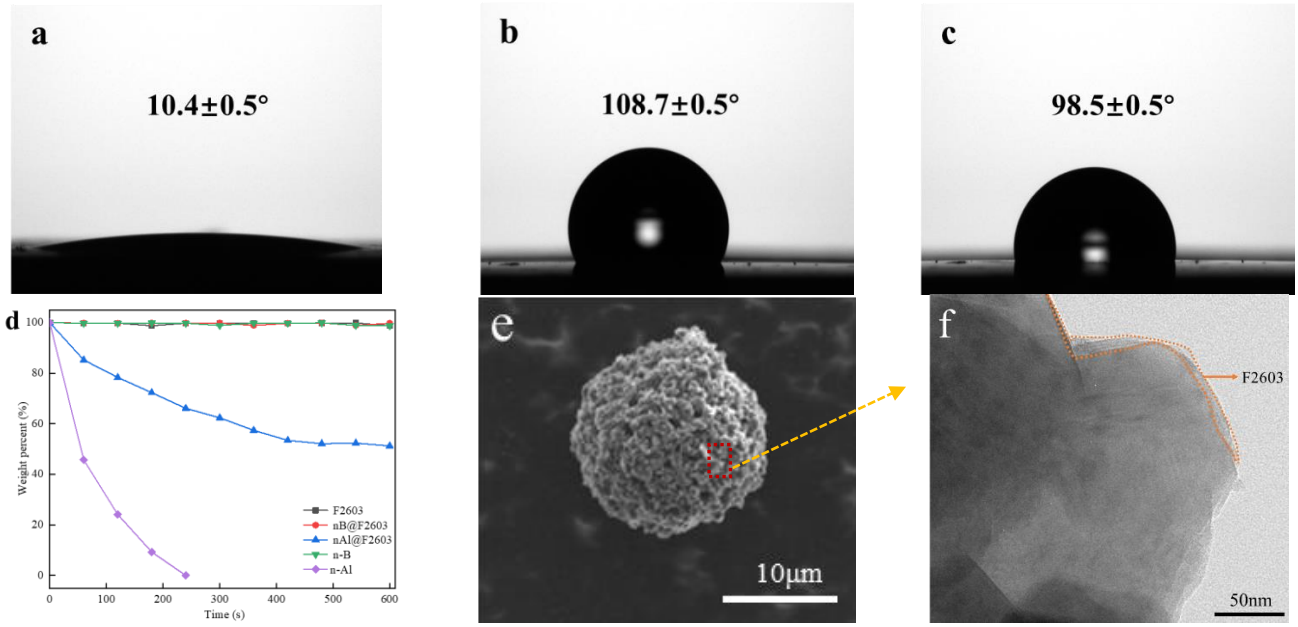

Figure 6. WCAs of (**a**) n-B, (**b**) F2603, and (**c**) nB@F2603 microspheres; (**d**) weight percentages of samples immersed in HCl solution for 10 min; (**e**) SEM images of nB@F2603 microspheres; (**f**) Local TEM images of nB@F2603 microspheres.

Since n-B hardly reacts with acid at room temperature, n-Al was used in place of n-B to evaluate the acid corrosion resistance of the microsphere structure. Figure 6d shows the weight loss curve of the n-Al@F2603 microspheres after their immersion in the HCl solution for 10 min. They exhibit a certain level of acid corrosion resistance; therefore, the nB@F2603 microspheres also have this property. Since F2603 is a corrosion-resistant, chemically stable polymer, it wraps the particle surfaces and forms a fibrous structure under the action of the high-voltage electric field. Most particles are embedded in the F2603 fibers, but some particles are not completely wrapped, resulting in weight loss.

3.3. Thermal Analysis

The thermal reaction performances of pure B and the microspheres were studied at a heating rate of 10 °C/min in air. The DSC–TG–DTG curves of the samples are shown in Figure 7. It can be seen from Figure 7 that the exothermic heat of the nB@F2603@CL-20 microspheres is divided into three stages. The first exothermic stage is caused by CL-20 decomposition, which releases gaseous products and other carbonaceous products. The TG and DTG curves show that CL-20 begins to decompose near 218.5 °C and reaches the maximum exothermic rate at 236.6 °C. The DSC curves show that the maximum exothermic peak of CL-20 decomposition is at 236.3 °C, which is slightly lower than the peak temperature of pure CL-20 [23]. This may be due to the change in the crystal form

of CL-20 caused by the electrospray process. The second exothermic stage corresponds to the decomposition of F2603, which starts at about 393.8 °C. The maximum decomposition rate is at 414.3 °C. The third exothermic stage is the most evident, namely, the oxidation exothermic reaction of n-B. According to the DSC–TG–DTG curves, the reaction starts at 521.1 °C, and the maximum reaction rate is achieved at 778.5 °C. The maximum exothermic peak temperature is 779.5 °C, which is slightly lower than the peak temperature of n-B. The peak temperature of the nB@F2603 microspheres is about 28 °C lower than the peak temperature of n-B. It is shown that the presence of F2603 and CL-20 promotes the oxidation of n-B. It can be seen from Figure 7b that the mass gain of the composite microspheres is obviously lower than that of n-B, which is apparently due to the low boron content in the composite microspheres. The mass gain of boron in composite microspheres was normalized by dividing the measured mass gain by boron content for comparison [24]. The normalized mass gain of n-B in the oxidation process is 128.2%. However, the normalized mass gain of the nB@F2603 microspheres and the nB@F2603@CL-20 microspheres is 139.2% and 143.6%, which is much higher than that of n-B. The significant increase in mass gain indicates the higher oxidation degree of the boron in composite microspheres.

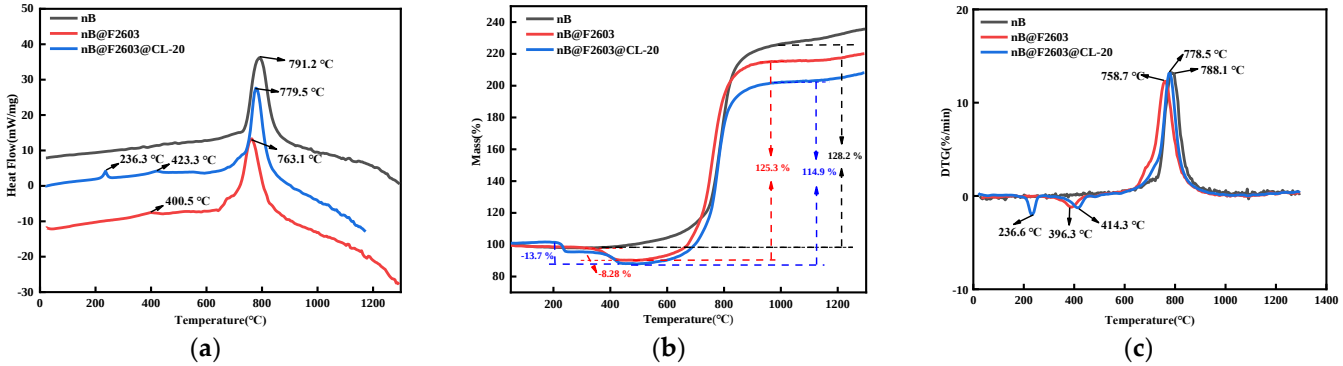

Figure 7. (**a**) DSC, (**b**) TG, and (**c**) DTG curves of n-B, nB@F2603 microspheres, and nB@F2603@CL-20 microspheres.

Considering the slow heating rate in the thermal analysis, the main reactions of each component in the microspheres are almost independent of each other. To explore the effects of F2603 and CL-20 on n-B, we studied and compared the kinetics of n-B and the nB@F2603 and nB@F2603@CL-20 microspheres in air by nonisothermal DSC–TG–DTG.

Figure 8 shows DSC curves of n-B (a), nB@F2603 (d), and nB@F2603@CL-20 (c) at different heating rates. Table 1 lists the peak temperatures of the samples at heating rates of 5 °C/min, 10 °C/min, 15 °C/min, and 20 °C/min. With the increase in heating rate, all peaks shift to the right. The apparent activation energy (Ea) of the exothermic peak of the sample is calculated by the Flynn–Wall–Ozawa method.

$$\ln \beta = \lg\left(\frac{AE_a}{RG(\alpha)}\right) - 2.315 - 0.4567\frac{E_a}{RT'} \quad (1)$$

where β is the heating rate (°C/min), T is the exothermic peak temperature in the DSC curve, α is the conversion ratio, $G(\alpha)$ is the integral model function, Ea is the apparent activation energy (J/mol), A is the pre-exponential factor (s–1), and R is the gas constant (8.314 J/[mol·K]).

A comparison of these Ea values indicates that the Ea value of the nB@F2603 microspheres is slightly higher than that of n-B, which may be due to the low thermal conductivity of F2603. When it coats the surface of n-B, it slightly prevents heat transfer, resulting in an increase in the activation energy of the nB@F2603 microspheres. However, the peak temperature of the n-B reaction in the nB@F2603 microspheres (Table 1) is lower than that of pure n-B, which is attributed to the chemical reaction between the decomposition product of F2603 and the oxide layer on the n-B surface. The Ea value of the nB@F2603@CL-20

microspheres is 13.25 kJ/mol lower than that of the nB@F2603 microspheres. This is because CL-20 is an energetic compound, and its crystallization in the pores of the microspheres can release energy during the reaction, thus accelerating the reaction rate and reducing the activation energy of the microspheres.

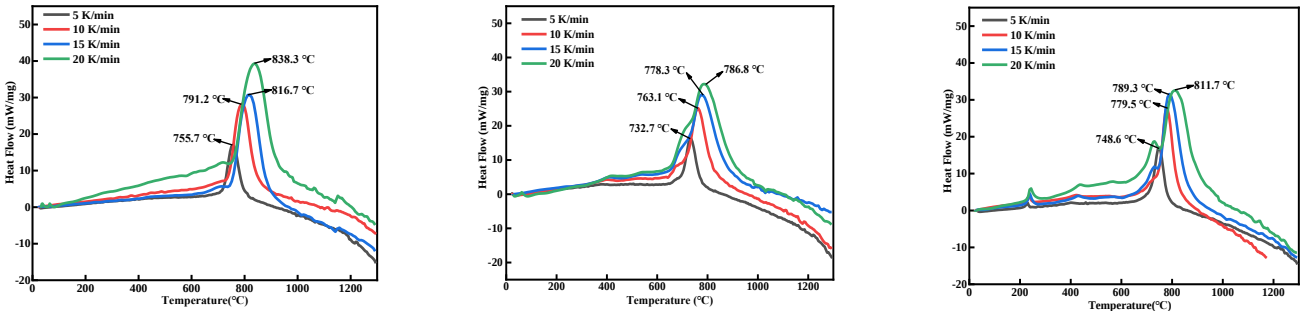

Figure 8. DSC curves of n-B (**a**), nB@F2603 (**b**), and nB@F2603@CL-20 (**c**) at different heating rates.

Table 1. Peak temperatures and kinetic parameters of samples.

Samples	Tp (°C)				*Ea* (kJ/mol)	r
	5	10	15	20		
nB	755.7	791.2	816.7	838.3	152.9	0.998
nB@F2603	732.7	763.1	778.3	786.8	211.7	0.996
nB@F2603@CL-20	748.6	779.5	789.3	811.7	198.5	0.986

The entire reaction of the nB@F2603@CL-20 microspheres was analyzed by TG-DTG-MS at a heating rate of 10 °C/min under an argon atmosphere. The TG-DTA-MS curves of the nB@F2603@CL-20 microspheres are shown in Figure 9c. It can be seen from the TG curve that there are two main weightless stages of the nB@F2603@CL-20 microspheres in argon atmosphere, namely the decomposition reaction of CL-20 and F2603. The ion current intensity of the MS signals and their possible decomposition gaseous products at the 431 °C are shown in Figure 9a. The large number of gaseous carbonaceous products detected by MS results indicates the rapid decomposition of the F2603 at this temperature. Moreover, there are some fluorine fragments in gaseous products since *m/z* signals of HF, CO_2, CF_2O F^+, C_2H_4, and CF_2 are detected. These fluorine fragments are strong oxidants and are favorable for the ignition and combustion of n-B [16]. It can be seen from Figure 9b that CL-20 decomposition mainly releases carbon-containing debris, while F2603 decomposition can decompose many fluorine-containing debris. Therefore, the decomposition of CL-20 has no effect on the reaction of n-B; it only affects the activation energy of the nB@F2603@CL-20 microspheres. The introduction of F2603 reduces the peak temperature of n-B, which is attributed to the fact that n-B promotes the decomposition of F2603, resulting in the generation of HF gas and F-containing fragments. These F-containing fragments react with the oxide layer on the boron surface to form BF_3 gas.

3.4. Ignition and Combustion Characteristics

We examined n-B and the nB@F2603 and nB@F2603@CL-20 microspheres using the MAC, constant-volume combustion cell, and laser ignition to explore the ignition and combustion properties of the nB@F2603@CL-20 microspheres.

The combustion heat of the samples was tested with the MAC, and the results are shown in Table 2. The amount of combustion heat reflects how much heat a sample can release from the combustion reaction. As seen in Table 2, the combustion heat value of the nB@F2603 microspheres increases slightly, and that of the nB@F2603@CL-20 microspheres rises by about 65%. The decomposition of CL-20 in the combustion process rapidly

generates large amounts of gas and heat in a short period of time, thereby promoting n-B combustion, that is, improving its combustion heat value.

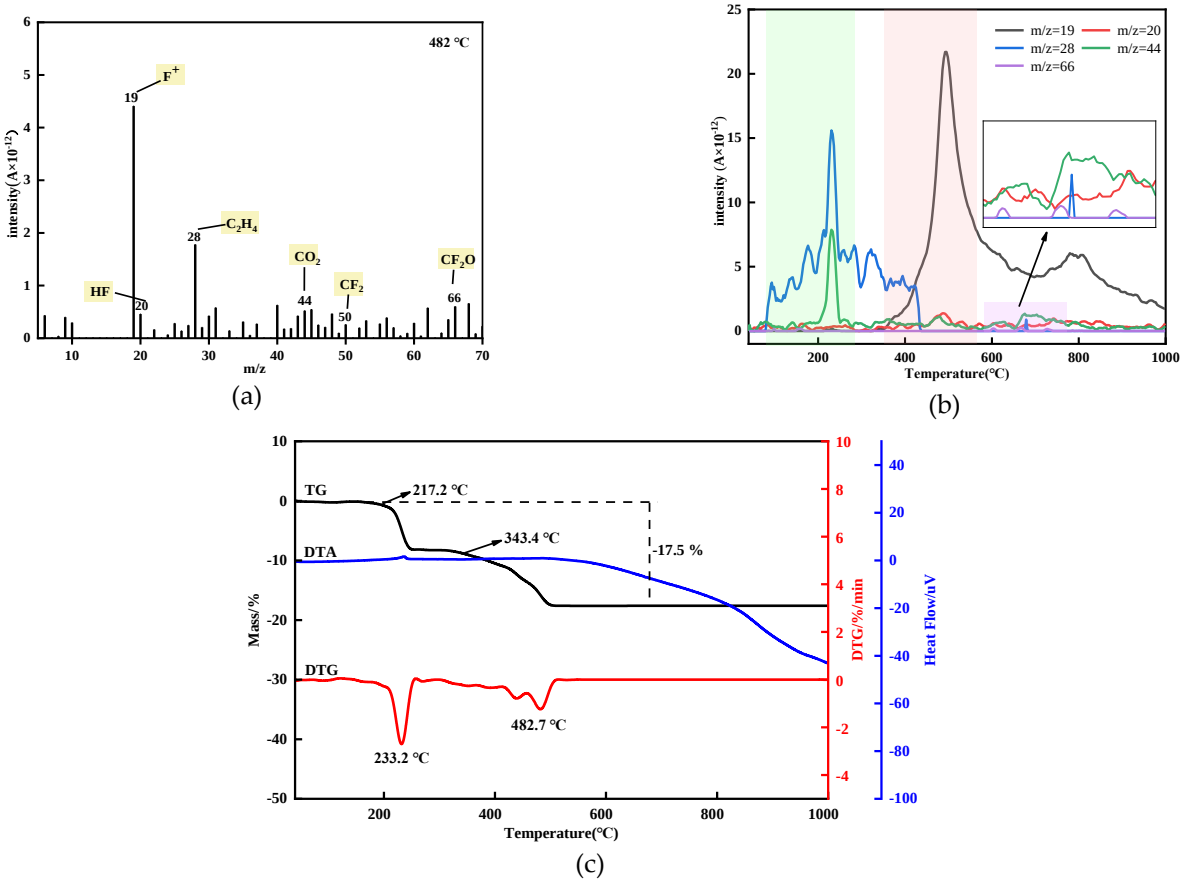

Figure 9. (**a**) Ionic current intensities of gaseous products that may be decomposed by nB@F2603@CL-20 microspheres at 482 °C; (**b**) ion MS at *m*/*z* = 19, 20, 28, 44, 66; (**c**) TG, DTA, and DTG curves of the nB@F2603@CL-20 microspheres at a heating rate of 10 °C/min under an argon atmosphere.

Table 2. Combustion heat value of n-B and nB@F2603 and nB@F2603@CL-20 microspheres.

Sample	n-B	nB@F2603 Microspheres	nB@F2603@CL-20 Microspheres
Experimental (kJ/g)	16.76 ± 0.02	20.63 ± 0.03	32.00 ± 0.02

The samples were subjected to an ignition test with CO_2 laser and a high-speed camera to explore the ignition delay time and combustion time of the nB@F2603@CL-20 microspheres. The test results are shown in Figure 10. Figure 10a shows the ignition and combustion processes of n-B. First, an evident spark is observed in the 11.6 ms image, indicating that n-B is ignited. Subsequently, n-B continues to burn; the flame is weak, accompanied by green light, and the combustion is not strong. A large number of unreacted solid particles are thrown out, and the whole process lasts about 260.2 ms. Figure 10b shows the ignition and combustion processes of the nB@F2603 microspheres. First, noticeable sparks are seen in the 3.5 ms image, suggesting that the nB@F2603 microspheres are ignited. Subsequently, the nB@F2603 microspheres continue to burn, accompanied by a layer of smoke caused by the decomposition of F2603. The whole combustion process lasts about 705.7 ms, and the combustion is highly intense. By contrast, the introduction of F2603 reduces the ignition delay time, prolongs the combustion, and makes the combustion reaction more intense and complete. The combustion of n-B produces many unreacted solid particles, and the combustion of nB@F2603 turns these particles into many bright

particles wrapped in smoke. F2603 reacts with the oxide layer on the n-B surface, hence promoting the ignition and combustion of n-B.

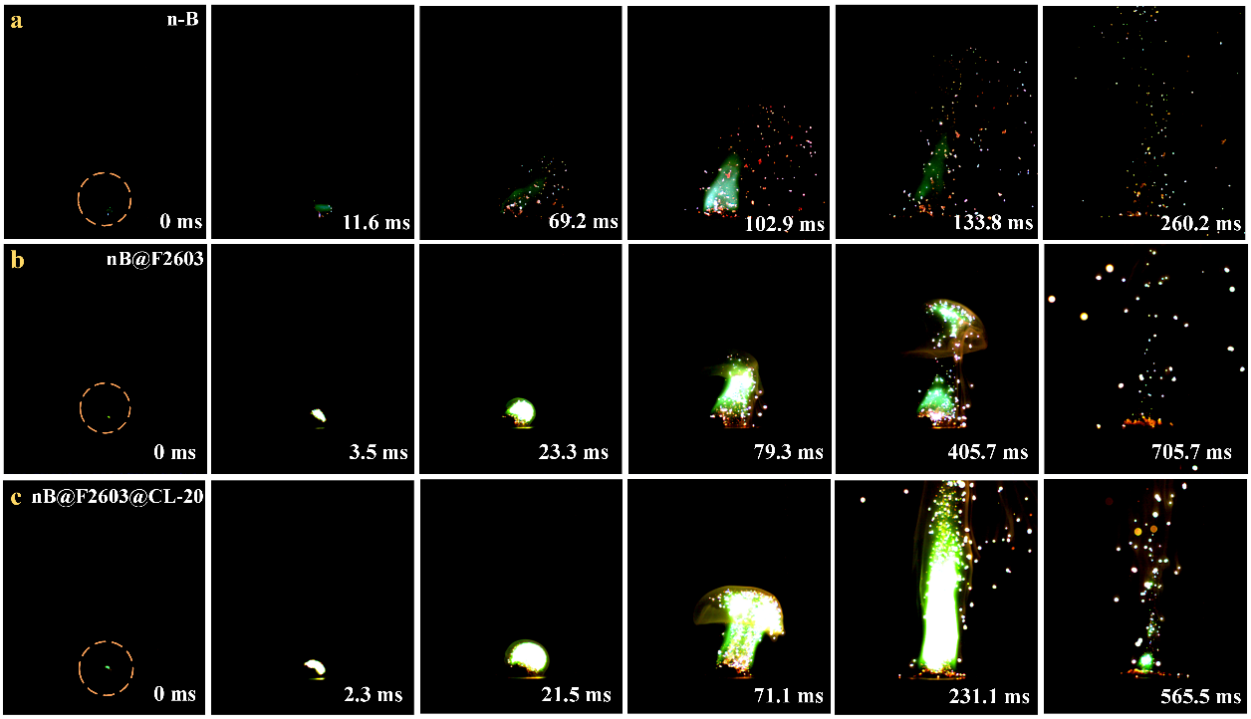

Figure 10. Ignition and combustion of (**a**) n-B, (**b**) nB@F2603 microspheres, and (**c**) nB@F2603@CL-20 microspheres in environment.

Figure 10c shows the ignition and combustion processes of the nB@F2603@CL-20 microspheres. The first visible flame is observed at 2.3 ms, indicating that the microspheres are ignited. The combustion process of the nB@F2603@CL-20 microspheres is very intense, and an obvious flame is seen in the diagram. The whole combustion process lasts about 565.5 ms. The introduction of CL-20 reduces the ignition delay, increases the combustion rate, and reduces the combustion time compared with those in Figure 10b. The decomposition of CL-20 has a significant effect on the ignition and combustion characteristics of the nB@F2603@CL-20 microspheres. This is due to the faster reaction rate of CL-20 during ignition and combustion, accompanied by the faster heating rate. The decomposition of CL-20 in the combustion process rapidly generates large quantities of gas and heat in a short period of time, which rapidly leads to the intense combustion of n-B.

Measurement of the pressure variation with time during combustion is an important means of characterizing the combustion performance of high-energy materials. The peak pressure that the high-energy material can achieve in the combustion process can be obtained from a pressure–time curve. The slope of this curve yields the pressurization rate in the initial reaction process, and the reaction rate of the high-energy material can then be characterized. The combustion performance of the samples was tested in a constant-volume combustion cell. The pressure trajectories of the microspheres and n-B are shown in Figure 11. The corresponding peak pressures and pressure rates are summarized in Table 3. The peak pressures of n-B, nB@F2603 microspheres, and nB@F2603@CL-20 microspheres are 64, 189.6, and 501.6 KPa, and their pressurization rates are 2.56, 4.99, and 15.19 MPa·s-1, respectively. The peak pressures of the assembled microspheres are remarkably better than that of n-B. Moreover, the introduction of CL-20 significantly increases the peak pressure and pressurization rate of the microspheres, which is consistent with the above ignition phenomenon.

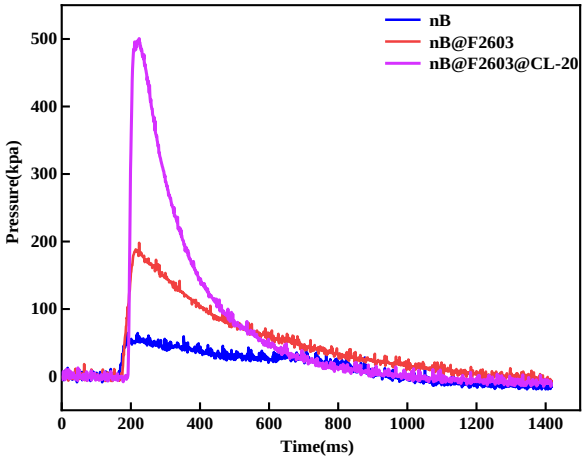

Figure 11. Pressure–time curves of n-B and nB@F2603 and nB@F2603@CL-20 microspheres under 1 MPa O_2.

Table 3. Maximum pressure (Pmax) and pressurization rate (dP/dt) of n-B and nB@F2603 and nB@F2603@CL-20 microspheres.

Sample	Pmax (KPa)	Pressurization Rate (MPa s^{-1})
n-B	64.0 ± 0.2	2.56 ± 0.03
nB@F2603 microspheres	189.6 ± 0.1	4.99 ± 0.02
nB@F2603@CL-20 microspheres	501.2 ± 0.1	15.19 ± 0.02

4. Conclusions

In summary, nB@F2603 and nB@F2603@CL-20 microspheres were successfully prepared by electrospray with F2603 as binder and CL-20 as high-energy filler. The particle size of the microspheres was found to be nearly 4 μm to 14 μm. Boron, fluorine, nitrogen, and CL-20 were uniformly distributed on the surface and the inside of the microspheres. F2603 was cross-linking materials, coating on the surfaces of the nano-boron and CL-20, and causing good hydrophobicity and acid corrosion resistance of the microspheres. A synergistic reaction between F2603 and nano-boron was found to accelerate the thermal decomposition, ignition, and combustion of the preagglomerated microspheres. HF gas and other fluorine-containing fragments generated by the decomposition of F2603 could react with the oxide shell on the surface of boron, forming gas BF_3. This reaction could reduce the initial ignition temperature of nano-boron and promote more violent combustion and energy release. The hydrophobicity and corrosion resistance tests showed that the preagglomeration microspheres had good stabilities. The degradation of CL-20 changes the reaction kinetics and contributes to the ignition and combustion of the reaction. Therefore, fluorine-containing nB@F2603 and nB@F2603@CL-20 microspheres might be used to replace nano-boron in composite energetic materials.

Author Contributions: Conceptualization, C.S. and S.Y.; methodology, J.Y.; investigation, Y.H. and K.C.; resource, J.N. and X.G.; data curation, J.Y.; writing—original draft preparation, J.Y.; writing—review and editing, S.Y. All authors have read and agreed to the published version of the manuscript.

Funding: This research was funded by the National Natural Science Foundation of China, grant numbers 21905024.

Data Availability Statement: Not applicable.

Conflicts of Interest: The authors declare no conflict of interest.

References

1. Dreizin, E.L. Metal-based reactive nanomaterials. *Prog. Energy Combust. Sci.* **2009**, *35*, 141–167. [CrossRef]
2. Wang, H.; Ren, H.; Yin, L.; Wu, X. High energy release boron-based material with oxygen vacancies promoting combustion. *Chem. Eng. J.* **2022**, *430*, 133027–133042. [CrossRef]
3. Ma, M.; Liu, G.; Qin, Z.; Zhang, R.; Ying, Y.; Xu, L.; Liu, D. Effects of aluminum addition on flash ignition and combustion of boron nanoparticles. *Combust. Flame* **2022**, *236*, 111762–111775. [CrossRef]
4. Chen, B.; Xia, Z.; Huang, L.; Hu, J. Ignition and combustion model of a single boron particle. *Fuel Process. Technol.* **2017**, *165*, 34–43. [CrossRef]
5. Liang, D.; Liu, J.; Zhou, Y.; Zhou, J. Ignition and combustion characteristics of amorphous boron and coated boron particles in oxygen jet. *Combust. Flame* **2017**, *185*, 292–300. [CrossRef]
6. Connell, T.L., Jr.; Yetter, R.A.; Risha, G.A.; Huba, Z.J.; Epshteyn, A.; TFisher, B. Enhancement of Solid Fuel Combustion in a Hybrid Rocket Motor Using Amorphous Ti-Al-B Nanopowder Additives. *J. Propuls. Power* **2019**, *35*, 662–665. [CrossRef]
7. Sun, Y.; Ren, H.; Du, F.; Yan, S.; Jiao, Q. Preparation and characterization of sintered B/MgB2 as heat release material. *J. Alloy. Compd.* **2018**, *759*, 100–107. [CrossRef]
8. Xu, S.; Chen, Y.; Chen, X.; Wu, D.; Liu, D. Combustion heat of the Al/B powder and its application in metallized explosives in underwater explosions, Combustion. *Explos. Shock. Waves* **2016**, *52*, 342–349. [CrossRef]
9. Chen, T.; Zhang, X.; Wang, Y.; Huang, L.; Xiao, J. Effect of LiF coating on the thermal oxidation characteristics for boron powder. *Chin. J. Energetic Mater.* **2013**, *21*, 57–60.
10. Gao, D.; Zhang, W.; Zhu, H.; Wang, C. Effect of coated and agglomerated boron on combustion characteristics of boron-based fuel-rich propellants. *J. Propuls. Technol.* **2009**, *30*, 119–123.
11. Keerthi, V.; Nie, H.; Pisharath, S.; Hng, H.H. Combustion characteristics of fluoropolymer coated boron powders. *Combust. Sci. Technol.* **2020**, *194*, 1183–1198. [CrossRef]
12. Bocanegra, P.E.; Chauveau, C.; Gökalp, I. Experimental studies on the burning of coated and uncoated micro and nano-sized aluminium particles. *Aerosp. Sci. Technol.* **2007**, *11*, 33–38. [CrossRef]
13. Yetter, R.A.; Risha, G.A.; Son, S.F. Metal Particle Combustion and Nanotechnology. *Proc. Combust. Inst.* **2009**, *32*, 1819–1838. [CrossRef]
14. Sumpter, B.G.; Beach, D.B.; Labinov, S.D.; Rondinone, A.J.; Richards, R.K. Solid-State Combustion of Metallic Nanoparticles: New Possibilities for an Alternative Energy Carrier. *J. Energy Resour. Technol.* **2007**, *129*, 29–32.
15. Bergthorson, J.M. Recyclable metal fuels for clean and compact zero-carbon power. *Prog. Energy Combust. Sci.* **2018**, *68*, 169–196. [CrossRef]
16. Cheng, L.; Huang, C.; Yang, Y.; Li, Y.; Artiaga, R. Preparation and combustion performance of B/PVDF/Al composite microspheres. *Propellants Explos. Pyrotech.* **2020**, *45*, 657–664. [CrossRef]
17. Wang, H.; Jian, G.; Yan, S.; Delisio, J.; Huang, C.; Zachariah, M. Electrospray formation of gelled nano-aluminum microspheres with superior reactivity. *ACS Appl. Mater. Interfaces* **2013**, *5*, 6797–6801. [CrossRef] [PubMed]
18. Young, G.; Wang, H.; Zachariah, M.R. Application of nano-aluminum/nitrocellulose mesoparticles in composite solid rocket propellants. *Propellants Explos. Pyrotech.* **2015**, *40*, 413–418. [CrossRef]
19. Wang, H.; Jian, G.; Egan, G.; Zachariah, M. Assembly and reactive properties of Al/CuO based nanothermite microparticles. *Combust. Flame* **2014**, *161*, 2203–2208. [CrossRef]
20. Wang, H.; Jacob, J.; DeLisio, B.; Michael, R. Assembly and encapsulation of aluminum NP's within AP/NC matrix and their reactive properties. *Combust. Flame* **2017**, *180*, 175–183. [CrossRef]
21. Wang, H.; Zachariah, R.; Xie, L.; Rao, G. Ignition and combustion characterization of nano-Al-AP and nano-Al-CuO-AP micro-sized composites produced by electrospray technique. *Energy Procedia* **2015**, *66*, 109–112. [CrossRef]
22. Anderson, S.R.; Dubé, P.; Krawiec, M.; Salan, J.S.; Ende, D.J. Promising CL-20-Based Energetic Material by Cocrystallization, Propellants. *Explos. Pyrotech.* **2016**, *41*, 783–788. [CrossRef]
23. Shi, Y.; Li, M.; Lu, S.; Jiao, Q.; Huang, R. Fabrication of Nano- and Micron- Sized Spheres of CL-20 by Electrospray. *Cent. Eur. J. Energetic Mater.* **2018**, *15*, 572–589.
24. Cheng, L.A.; Yang, H.B.; Yang, Y.A.; Li, Y.A.; Meng, Y.A.; Li, Y.A. Preparation of B/Nitrocellulose/Fe particles and their effect on the performance of an ammonium perchlorate propellant. *Combust. Flame* **2020**, *211*, 456–464. [CrossRef]